HHS Public Access

Author manuscript

Neurobiol Aging. Author manuscript; available in PMC 2023 September 01.

Published in final edited form as:

Neurobiol Aging. 2022 September ; 117: 128–138. doi:10.1016/j.neurobiolaging.2022.05.009.

Limbic-predominant age-related TDP-43 encephalopathy neuropathological change (LATE-NC) is associated with lower R_2 relaxation rate: An ex-vivo MRI and pathology investigation

Mahir Tazwar[a], **Arnold M. Evia**[b], **Ashish A. Tamhane**[b], **Abdur Raquib Ridwan**[a], **Sue E. Leurgans**[b,c], **David A. Bennett**[b,c], **Julie A. Schneider**[b,c,d], **Konstantinos Arfanakis**[a,b,e]

[a]Department of Biomedical Engineering, Illinois Institute of Technology, Chicago, Illinois, USA.

[b]Rush Alzheimer's Disease Center, Rush University Medical Center, Chicago, Illinois, USA.

[c]Department of Neurological Sciences, Rush University Medical Center, Chicago, Illinois, USA.

[d]Department of Pathology, Rush University Medical Center, Chicago, Illinois, USA.

[e]Department of Diagnostic Radiology, Rush University Medical Center, Chicago, Illinois, USA.

Abstract

Limbic predominant age-related transactive response DNA binding protein 43 (TDP-43) encephalopathy neuropathological change (LATE-NC) is common in persons older than 80 years of age and is associated with cognitive decline and increased likelihood of dementia. The MRI signature of LATE-NC has not been fully determined. In this study, the association of LATE-NC with the transverse relaxation rate, R_2, was investigated in a large number of community-based older adults. Cerebral hemispheres from 738 participants of the Rush Memory and Aging Project, Religious Orders Study, and Minority Aging Research Study, were imaged ex-vivo with multi-echo spin-echo MRI and underwent detailed neuropathologic examination. Voxel-wise analysis revealed a novel spatial pattern of lower R_2 for higher LATE-NC stage, controlling for other neuropathologies and demographics. This pattern was consistent with the distribution of LATE-

Correspondence to: Konstantinos Arfanakis, PhD, 1750 W Harrison, Suite 1000, Chicago, IL 60612, Phone: (312) 942-6377, konstantinos_arfanakis@rush.edu.

Author contributions

Conceptualization: MT, JAS, KA. Data curation: AME, AAT, SEL, DAB, JAS, KA. Formal analysis: MT, AME, SEL, KA. Funding acquisition: DAB, JAS, KA. Investigation: MT, JAS, KA. Methodology: MT, AME, ARR, SEL, JAS, KA. Project administration: KA. Resources: SEL, DAB, JAS, KA. Software: MT, AME, ARR. Supervision: KA. Validation: MT, AME, ARR, SEL, KA. Visualization: MT, KA. Writing - original draft: MT, KA. Writing - review & editing: MT, AME, AAT, ARR, SEL, DAB, JAS, KA.

Conflict of interest statement

The authors have no financial interests or relationships to disclose with regard to the subject matter of this manuscript.

Data

The data contained in the manuscript have not been previously published, have not been submitted elsewhere and will not be submitted elsewhere while under consideration at Neurobiology of Aging.

Human subjects

All participants provided written informed consent and signed an anatomical gift act.

Authors

All authors have reviewed the contents of the manuscript, approve of its contents and validate the accuracy of the data.

NC in gray matter, and also involved white matter providing temporo-temporal, fronto-temporal, and temporo-basal ganglia connectivity. Furthermore, analysis at different LATE-NC stages showed that R_2 imaging may capture the general progression of LATE-NC, but only when TDP-43 inclusions extend beyond the amygdala.

Keywords

MRI; R_2; ex-vivo; pathology; limbic predominant age-related TDP-43 encephalopathy neuropathological change (LATE-NC); transactive response DNA binding protein of 43kDa (TDP-43)

1. Introduction

Limbic-predominant age-related transactive response DNA binding protein 43 (TDP-43) encephalopathy neuropathological change (LATE-NC) is characterized by the accumulation of TDP-43 proteinopathy primarily in limbic structures of the brain of older adults with or without coexisting hippocampal sclerosis (Nelson et al., 2019). LATE-NC is common in persons older than 80 years of age and is observed in more than 20% of brains at autopsy (Nelson et al., 2019). LATE-NC often coexists with Alzheimer's disease (AD) (Arai et al., 2009; Tremblay et al., 2011), Lewy body pathology (Arai et al., 2009), argyrophilic grains (Fujishiro et al., 2009), hippocampal sclerosis (Amador-Ortiz et al., 2007; Zarow et al., 2012), as well as with microvascular pathologies such as arteriolosclerosis (Agrawal et al., 2021a), but it is also found in brains without other significant pathology (Arnold et al., 2013; Geser et al., 2010; McAleese et al., 2017; Uchino et al., 2015; Wilson et al., 2013). It is now well-established that LATE-NC is associated with cognitive decline, particularly in episodic memory (Wilson et al., 2013), and increased likelihood of dementia above and beyond the contributions of other age-related neuropathologies (Josephs et al., 2014; Kawas and Corrada, 2006; Nelson et al., 2019; Tremblay et al., 2011). Moreover, LATE-NC has been shown to account for nearly as much of the variance in late-life cognitive decline as neurofibrillary tangles (hallmark pathology of AD) (Wilson et al., 2013). Over the past decade, few studies combining structural magnetic resonance imaging (MRI) and pathology information have demonstrated that LATE-NC is associated with atrophy in the medial temporal lobe (Bejanin et al., 2019; Buciuc et al., 2020; Dawe et al., 2011; Josephs et al., 2016, 2014; Makkinejad et al., 2019; Nelson et al., 2019) and frontal lobe (Bejanin et al., 2019; Josephs et al., 2016; Nelson et al., 2019). However, despite these few studies on brain atrophy, the association of LATE-NC with other brain MRI characteristics has not been investigated. Therefore, the MRI signature of LATE-NC remains largely undetermined.

The transverse relaxation rate, R_2, the reciprocal of the transverse relaxation time T_2, is one of the main sources of contrast in MRI (Brown et al., 2014). R_2 describes the rate of decay of transverse magnetization due to irreversible dephasing and is sensitive to myelin breakdown, neuronal loss, increased water content, and increased iron concentration (Bartzokis et al., 2003; Haacke et al., 2005; House et al., 2008). R_2-weighted images are collected in practically all clinical MRI scans and R_2 has been used to study a wide range of diseases. Previous work combining MRI and pathology in older adults has shown that

Alzheimer's and vascular pathologies are associated with lower R_2 in white matter of all lobes due to myelin breakdown, neuronal loss, and increased water content, and that Alzheimer's pathology is also associated with higher R_2 in basal ganglia due to elevated iron concentrations (Besson et al., 1992; Dawe et al., 2014; House et al., 2008). However, no prior studies have investigated the association of LATE-NC with R_2.

In this cross-sectional study, we tested the hypothesis that LATE-NC is associated with lower R_2 and extracted the spatial pattern of LATE-NC-related R_2 abnormalities by combining ex-vivo MRI and pathology in a large community-based cohort of older adults. Cerebral hemispheres from 738 participants of the Rush Memory and Aging Project, the Religious Orders Study, and the Minority Aging Research Study were imaged ex-vivo with multi-echo spin-echo MRI and underwent detailed neuropathologic examination. MRI was conducted ex-vivo to ensure that no additional pathology could develop between imaging and autopsy. A cerebrum-wide voxel-wise analysis was used to extract the spatial pattern of the independent association of ex-vivo R_2 with LATE-NC controlling for other neuropathologies and demographics. We also identified the gray matter regions and white matter connections exhibiting the strongest link between R_2 and LATE-NC. Finally, we investigated R_2 abnormalities at different LATE-NC stages and identified the earliest stage exhibiting statistically significant R_2 anomalies.

2. Methods

2.1. Study Population

Participants in three longitudinal, epidemiologic, clinical-pathologic cohort studies of aging, the Rush Memory and Aging Project (MAP), the Religious Orders Study (ROS) (Bennett et al., 2018), and the Minority Aging Research Study (MARS) (Barnes et al., 2013) were included in this work. The three studies were approved by the institutional review board of Rush University Medical Center. All participants provided written informed consent to undergo annual uniform structured clinical evaluations including cognitive function testing, medical history, and neurologic examination (Bennett et al., 2006). Clinical diagnosis of dementia followed the criteria established by the National Institute of Neurological and Communicative Disorders and Stroke and the Alzheimer's Disease and Related Disorders Association (McKhann et al., 1984). Participants who did not meet the criteria for dementia in spite of having cognitive impairment were classified as having mild cognitive impairment (MCI) (Bennett et al., 2002; Boyle et al., 2006), whereas subjects without dementia or MCI were classified as no cognitive impairment (NCI). All MAP and ROS participants and a subset of MARS participants signed an anatomical gift act for brain donation at death. At the time of these analyses, 5062 participants of the parent projects had completed the baseline clinical evaluation. Of these, 620 were deceased and 123 withdrew from the studies before the ex-vivo MRI sub-study began. Of the remaining 4319 participants, 1557 died, 1263 were autopsied, and 1024 had ex-vivo MRI and pathology data. The first 738 consecutive participants with ex-vivo MRI data that passed quality tests and complete neuropathologic evaluations who did not have frontotemporal lobar degeneration (FTLD, N=4) were considered in this work (Table 1).

2.2. Brain hemisphere preparation

At autopsy, a technician removed the brain and separated the cerebrum from the cerebellum and brainstem. The cerebrum was then bisected and a hemisphere, with more visible pathology if applicable, was selected for ex-vivo MRI and gross pathologic examination, while the contralateral hemisphere was frozen and stored. The hemisphere chosen for imaging was fixed in phosphate-buffered 4% formaldehyde solution and refrigerated at 4°C in a sealed plastic container within 30 minutes of removal from the skull. Ex-vivo MRI was conducted at room temperature, while the hemisphere was immersed in formaldehyde solution with its medial aspect facing the bottom of the container (Arfanakis et al., 2020; Kotrotsou et al., 2015) (ex-vivo MRI methods can be found in Section 2.3). Gross examination was performed within two weeks after ex-vivo MRI, followed by histopathologic diagnostic examination (Kotrotsou et al., 2015) (histopathologic examination is described in Section 2.4).

2.3. Ex-vivo MRI acquisition and R_2 quantification

Cerebral hemispheres were imaged ex-vivo on 3 Tesla clinical MRI scanners using 2D multi-echo spin-echo (ME-SE) sequences, approximately one month postmortem to allow for stabilization of R_2 values (Dawe et al., 2009). Due to the ongoing nature of the studies and scanner upgrades, four different scanners were used in this work. Nevertheless, the ME-SE protocols in all scanners had the same acquired voxel-size (0.6mm × 0.6mm × 1.5mm), had echo times that covered the range of approximately 10ms – 50ms (the T_2 value of brain tissue immersed in formaldehyde solution for about one month is approximately half of that in-vivo), and the same total scan time of approximately 30 minutes (more details on the imaging protocols can be found in Arfanakis et al., 2020).

For each hemisphere, the transverse relaxation rate R_2 was quantified in each voxel by fitting a mono-exponential decay function $S = S_0 \cdot \exp(-R_2 \cdot t)$ to the ME-SE data using a least squares approach, where S is the signal of a voxel at time t, and S_0 is the signal at t = 0 ms. The images from the first echo of the ME-SE data were non-linearly registered to an ex-vivo MRI brain hemisphere template using ANTs (Avants et al., 2011). The resulting spatial transformations were applied to the corresponding R_2 maps to bring them into a common space and facilitate voxel-wise analyses (Dawe et al., 2016, 2014).

2.4. Neuropathologic evaluation

Following ex-vivo MRI, each hemisphere was sectioned into 1-cm thick coronal slabs. The slabs were evaluated macroscopically, and selected tissue blocks were dissected, embedded into paraffin, cut into sections, and mounted on glass slides (more details on these well-established procedures are provided in Schneider et al., 2003). LATE-NC was assessed using immunohistochemistry to detect abnormal TDP-43 cytoplasmic inclusions (Nag et al., 2015) in the amygdala, entorhinal cortex, hippocampus (dentate gyrus and CA1 sector), midfrontal cortex, middle temporal cortex, temporal pole, and inferior orbitofrontal cortex. LATE-NC was summarized into 4 stages: stage 0 (no TDP-43 inclusions), stage 1 (TDP-43 inclusions in amygdala only), stage 2 (TDP-43 inclusions in amygdala and entorhinal cortex or hippocampus), stage 3 (TDP-43 inclusions in amygdala, entorhinal cortex or hippocampus, and neocortex) (Nelson et al., 2019). AD neuropathological change

was ranked using the ABC score incorporating assessments of amyloid β deposits in 7 brain regions (midfrontal, middle temporal, inferior parietal, and cerebellar cortices, hippocampus, basal ganglia, substantia nigra) and described by a modified version of Thal phases (A score: 0, 1, 2, 3), staging of neurofibrillary tangles (NFT) (in hippocampus, entorhinal, midfrontal, inferior parietal, middle temporal cortices) modified from Braak and Braak (B score: 0, 1, 2, 3), and scoring of neuritic plaques (in midfrontal, inferior parietal, middle temporal cortices) modified from the Consortium to Establish a Registry for AD (CERAD) (C score: 0, 1, 2, 3) (Hyman et al., 2012). A pathologic diagnosis of AD was also rendered using the National Institute on Aging-Alzheimer's Association (NIA-AA) criteria (Hyman et al., 2012). Lewy bodies were evaluated in 7 brain regions (midfrontal, middle temporal, inferior parietal, entorhinal, and anterior cingulate cortices, amygdala, and substantia nigra) and were rated as absent or present (Agrawal et al., 2021b). Gross infarcts visible to the naked eye were rated as 0 (none), 1 (one), or 2 (more than one) (Schneider et al., 2003). Microscopic infarcts were identified in 6μm H&E (hematoxylin and eosin) stained sections from a minimum of 9 regions (midfrontal, middle temporal, entorhinal, hippocampal and inferior parietal cortices, anterior cingulate, thalamus, basal ganglia and midbrain) and were also rated as 0 (none), 1 (one), or 2 (more than one) (Arvanitakis et al., 2017). Cerebral amyloid angiopathy (CAA) was assessed in 4 regions (midfrontal, middle temporal, angular and calcarine cortices) and was scored as none, mild, moderate, and severe (Boyle et al., 2015). Atherosclerosis was detected based on the quantity and degree of vascular involvement at the circle of Willis and was rated as none, mild, moderate, and severe (Arvanitakis et al., 2016). Arteriolosclerosis was identified based on the severity of wall thickening and luminal occlusion of the small arterioles in sections of the anterior basal ganglia (anterior caudate, putamen, globus pallidus and internal capsule) and was ranked as none, mild, moderate, and severe (Arvanitakis et al., 2016).

2.5. Statistical analysis

First, voxel-wise linear regression using a non-parametric permutation test was used to analyze the association of R_2 relaxation rate (dependent variable) with LATE-NC stage (independent variable) or each of the other neuropathologies separately (A, B, C scores for AD neuropathological change, the presence of Lewy bodies, the ordinal variables for gross and microscopic infarcts, and the severity of CAA, atherosclerosis, and arteriolosclerosis; all were summary measures, not specific to individual brain regions), controlling for demographics (age at death, sex, and education), scanner, postmortem interval to fixation (PMI_f), and postmortem interval to imaging (PMI_i). Next, voxel-wise linear regression using a non-parametric permutation test was used to analyze the association of R_2 relaxation rate with LATE-NC stage controlling for all other neuropathologies that generated significant findings in the single pathology models described above, and also controlling for demographics, scanner, PMI_f, and PMI_i. The above analyses were conducted using PALM (FSL, FMRIB, Oxford, UK) (Winkler et al., 2014) with 10,000 permutations, threshold-free cluster enhancement, and family-wise error rate (FWER) correction. Associations were considered significant in voxels with a corrected $p<0.05$.

The strength of the association of R_2 with LATE-NC was evaluated in gray and white matter. First, gray matter structures demonstrating the strongest association according to the voxel-

wise analysis were identified using the gray matter labels of the IIT Human Brain Atlas v.5.0 (Qi and Arfanakis, 2021) as a reference. Second, the strength of the association of R_2 with LATE-NC in white matter fibers of the brain structural connectome was assessed using an atlas-based approach. More specifically, the ex-vivo MRI brain hemisphere template that was used as a reference in the voxel-wise analysis was first non-linearly registered to the left hemisphere of the IIT Human Brain Atlas v.5.0 using ANTs (Avants et al., 2011), and the resulting spatial transformations were applied to the coefficient map generated in the voxel-wise analysis to transform it to atlas space. All tract density images (TDI) of the IIT Human Brain Atlas, defining the connectivity between all possible pairs of gray matter labels of the atlas, were thresholded at 5% of the maximum number of streamlines per TDI, thereby generating a mask for each connection. The coefficients from the voxel-wise analysis that were located inside each mask were averaged into a single number per mask to represent the strength of the association of R_2 with LATE-NC in the corresponding white matter connection. A connectivity matrix was then constructed including the strength of the association of R_2 with LATE-NC in different association and projection fibers of the brain. Commissural fibers were not included because ex-vivo MRI was conducted in a single cerebral hemisphere from each participant.

R_2 differences in LATE-NC stages 1, 2, 3 compared to LATE-NC stage 0 were investigated in brain regions that showed significant associations of R_2 with LATE-NC in the voxel-wise analysis. These regions were manually defined (once) in the space of the ex-vivo MRI brain hemisphere template that was used as a reference in the voxel-wise analysis. For each hemisphere, the median R_2 value was determined in each region separately. Linear regression with a non-parametric permutation test was used in each region to test for significantly lower regional R_2 in LATE-NC stages 1, 2, 3 compared to LATE-NC stage 0 controlling for other neuropathologies, demographics, scanners, and postmortem intervals. These analyses were conducted using PALM and differences were considered significant when $p<0.05$ after FWER correction.

3. Results

3.1. Demographic, clinical, and neuropathologic characteristics

Among the 738 community-based older adults considered in this study, 72% were female, 93% were white and 6% black (Table 1). At the last evaluation conducted 0.7 years (median) prior to death, 31% of the participants had no cognitive impairment (NCI), 23% had mild cognitive impairment (MCI), and 47% had dementia. The mean age at death was 90.6 years (SD = 6.4 years, range = 66–108 years), and the mean postmortem interval to fixation was 9.9 hours (SD = 7.8 hours). Neuropathologic evaluation showed that 57% of the participants had LATE-NC, and 74% had intermediate or high AD neuropathological change (Table 2).

3.2. Association of R_2 with LATE-NC

The voxel-wise analysis demonstrated lower R_2 values for higher LATE-NC stage in a spatial pattern involving regions of the temporal, frontal, occipital lobes and basal ganglia (FWER corrected $p<0.05$) (controlling for all pathologies other than microscopic infarcts which were not associated with R_2 in the single pathology models) (Fig. 1). The strongest

effects in gray matter were observed in the amygdala, hippocampus, parahippocampal cortex, entorhinal cortex, and temporal pole, followed by the inferior insula, inferior putamen, fusiform, nucleus accumbens, and medial orbitofrontal cortex. Weaker yet significant associations of lower R_2 values with higher LATE-NC stage were found in the inferior, middle and superior temporal cortices, caudate, rostral anterior cingulate cortex, superior frontal cortex, lingual cortex, and lateral occipital cortex. Much of the spatial pattern produced by the voxel-wise analysis involved white matter, and the strength of the association of R_2 with LATE-NC per white matter connection of the brain structural connectome is shown in the connectivity matrix of Figure 2. This symmetric heatmap includes three distinct clusters indicating that temporo-temporal, fronto-temporal, and temporo-basal ganglia connections exhibited the most negative association of R_2 values with LATE-NC (Fig. 2). Temporo-occipital and temporo-parietal connections were less involved, and so were connections of the frontal lobe and basal ganglia to non-temporal regions. Connections between regions of the parietal lobe and any other brain region exhibited the weakest associations between R_2 values and LATE-NC. Finally, no gray or white matter region showed positive associations of R_2 values with LATE-NC (Fig. 1).

3.3. R_2 abnormalities in different LATE-NC stages

The regions of interest (ROI) that were selected to investigate R_2 differences in LATE-NC stages 1, 2, 3 compared to stage 0 included the amygdala, hippocampus, parahippocampal white matter, temporal pole white matter, temporal lobe white matter, inferior insular white matter, medial orbitofrontal white matter, and occipitotemporal cortex, and are displayed in Figure 3A. An additional ROI in the parietal lobe that showed no association of R_2 with LATE-NC in the voxel-wise analysis was also selected for reference (Fig. 3A). In general, later stages of LATE-NC exhibited lower R_2 values in all ROIs other than the parietal ROI where the R_2 remained rather constant (Fig. 3B), as expected based on the voxel-wise analysis. No significant difference was observed in R_2 for LATE-NC stage 1 compared to stage 0 in any of the ROIs (Table 3). Significantly lower R_2 for LATE-NC stage 2 compared to stage 0 was observed in the amygdala, hippocampus, parahippocampal white matter, and temporal pole white matter ($p<0.05$, FWER-corrected) (Table 3). Significantly lower R_2 for LATE-NC stage 3 compared to stage 0 was observed in the amygdala, hippocampus, parahippocampal white matter, temporal pole white matter, temporal lobe white matter, insular white matter, medial orbitofrontal white matter, and occipitotemporal cortex ($p<0.05$, FWER-corrected) (Table 3).

4. Discussion

The present study tested the hypothesis that LATE-NC is associated with lower transverse relaxation rate R_2 and extracted the spatial pattern of LATE-NC-related R_2 abnormalities, by combining ex-vivo MRI and detailed pathologic evaluation in a large community-based cohort of older adults. Voxel-wise analysis demonstrated lower R_2 values for higher LATE-NC stage in a spatial pattern involving gray matter regions of the temporal, frontal, occipital lobes and basal ganglia, and white matter providing temporo-temporal, fronto-temporal, and temporo-basal ganglia connectivity. The extracted spatial pattern may be used in combination with other information to develop tools for in-vivo detection of this devastating

neuropathology which, currently, can only be diagnosed at autopsy. Furthermore, in the present study, LATE-NC-related R_2 anomalies became statistically significant in stage 2 in the amygdala, hippocampus, parahippocampal white matter, and temporal pole white matter, and extended to more regions of the temporal, frontal, and occipital lobes, and basal ganglia in stage 3. This suggests that R_2 imaging may capture the general progression of LATE-NC, but the earliest impact of the pathology on R_2 is detected when TDP-43 inclusions extend beyond the amygdala. R_2 is one of the main sources of contrast in MRI, and to our knowledge this is the first study to investigate the R_2 signature of LATE-NC.

The independent association of lower R_2 values with higher LATE-NC stage presented in this work is in good agreement with the neurobiological sequelae of this pathology. LATE-NC is associated with neuronal dropout and astrocytosis (Amador-Ortiz and Dickson, 2008; Nelson et al., 2019). Myelin breakdown and neuronal degeneration have been shown to increase water content in brain tissue (Bartzokis et al., 2003). Since the R_2 of water is tens of times lower than that of brain tissue, LATE-NC-associated neuronal damage can lower R_2 values as shown in the present work. Lower R_2 values were also observed previously following neurodegeneration associated with Alzheimer's pathology (Bartzokis et al., 2003; Besson et al., 1992; Dawe et al., 2014; House et al., 2008).

The spatial pattern of LATE-NC-related R_2 abnormalities revealed in the voxel-wise analysis exhibits an outstanding agreement with the pattern of TDP-43 deposition seen in pathologic studies of LATE-NC. We observed lower R_2 values for higher LATE-NC stage in the amygdala, hippocampus, parahippocampal cortex, entorhinal cortex, temporal pole, inferior insula, inferior putamen, fusiform, nucleus accumbens, medial orbitofrontal cortex, inferior, middle and superior temporal cortices, caudate, rostral anterior cingulate cortex, superior frontal cortex, lingual cortex, and lateral occipital cortex, and these are the same regions having TDP-43 inclusions in different stages of LATE-NC according to pathologic studies (Josephs et al., 2019, 2016; Nag et al., 2018; Nelson et al., 2019). This spatial pattern appeared more continuous and robust in subcortical gray and white matter and somewhat noisy in parts of the cortex only due to the well-known fact that the accuracy of spatial normalization across hemispheres is lower in parts of the cortex, even for state-of-the-art image registration methods such as the one used here. MRI-based brain morphometry and FDG-PET studies of LATE-NC have also used voxel-wise analyses and have revealed patterns of LATE-NC-related atrophy mainly in medial temporal lobe regions and hypometabolism in medial temporal and frontal lobe regions (Bejanin et al., 2019; Buciuc et al., 2020; Josephs et al., 2014). Overall, R_2 mapping captures well the spatial signature of LATE-NC and may be used in combination with other imaging modalities to develop tools for in-vivo prediction of this devastating neuropathology (see Appendix A for an example of LATE-NC classification based exclusively on R_2).

The structural connectome-based analysis demonstrated that the most negative associations of R_2 with LATE-NC were located in temporo-temporal, fronto-temporal, and temporo-basal ganglia connections, indicating that the greatest impact of the disease in white matter occurs in connections between gray matter regions with the highest TDP-43 burden. A plausible explanation may be that axonal degeneration secondary to TDP-43 inclusions may be more widespread in white matter dominated by connections to gray matter regions with high

TDP-43 burden. Although the exact pathobiologic mechanism underlying the propagation of TDP-43 in the brain remains elusive, it has been hypothesized that LATE-NC propagates through synaptically connected cells exhibiting a “prion-like” behavior, much like what is hypothesized about the spread of tau and α-synuclein (Goedert et al., 2014). Our finding emphasizes that the gray matter regions typically affected by LATE-NC are nodes of a well-connected network, and that the impact of the disease can be seen in both the nodes and edges of this network.

The ROI investigation of R_2 differences in LATE-NC stages 1, 2, 3 compared to stage 0 showed the earliest detectable R_2 abnormalities in the amygdala, hippocampus, parahippocampal white matter, and temporal pole white matter in stage 2, and additional R_2 abnormalities in other parts of the temporal, frontal and occipital lobes in stage 3. Previous pathologic studies of LATE-NC have shown that TDP-43 inclusions are first detected and are most common in the amygdala in stage 1, and progress to the hippocampus or entorhinal cortex in stage 2 (James et al., 2016; Josephs et al., 2016; Nelson et al., 2019). Thus, according to our findings, R_2 is sensitive to tissue anomalies in the regions affected first by LATE-NC, but R_2 abnormalities in the amygdala are somewhat delayed and appear in stage 2, after TDP-43 inclusions can be found outside the amygdala. This suggests that the impact of TDP-43 inclusions on amygdalar tissue integrity as measured by R_2 may be somewhat limited in stage 1 and becomes more substantial in stage 2. Interestingly, cognitive changes associated with LATE-NC are also detectable starting at stage 2, after TDP-43 inclusions extend beyond the amygdala (James et al., 2016). On the other hand, recent MRI volumetric work has shown significantly lower amygdala volume beginning in stage 1, a finding that was however accompanied by significantly lower entorhinal and hippocampal volume also in stage 1, before TDP-43 inclusions can be detected in the latter two regions (Bejanin et al., 2019). In addition to the amygdala, hippocampus and parahippocampal white matter, temporal pole white matter also showed the earliest detectable R_2 abnormalities in LATE-NC stage 2 (Table 3). This is in good agreement with previous work showing that TDP-43 deposition in the temporal pole is an early neocortical stage of LATE-NC progression, before TDP-43 is deposited in other neocortical areas (Nag et al., 2018). Finally, the R_2 of ROIs in the temporal lobe, insular, and medial orbitofrontal white matter, and occipitotemporal cortex was lower in stage 3 compared to stage 0, in agreement with the findings of pathologic studies that have shown these parts of the brain to be involved later in the progression of the disease (Josephs et al., 2016; Nag et al., 2018; Nelson et al., 2019). Overall, the ROI investigation of R_2 differences in stages 1, 2, 3 compared to stage 0 provided evidence that R_2 imaging may capture the general progression of LATE-NC.

This work has important strengths and also a few limitations. First, the use of MRI and pathology data from a large number of community-based older adults provided excellent statistical power and enhanced generalizability of findings. Second, detailed pathologic evaluation allowed us to investigate the independent effects of LATE-NC on R_2 by regressing out the effects of comorbid pathologies. Third, use of ex-vivo instead of in-vivo MRI ensured that imaging captures brain characteristics at the same LATE-NC stage as neuropathologic examination, which is important especially for studying R_2 abnormalities at different stages of the disease. Ex-vivo MRI also allowed imaging independent of frailty

level thereby increasing generalizability of findings. We expect the ex-vivo MRI findings to hold in-vivo as we have already demonstrated that for the same tissue preparation and imaging protocol as those used here, ex-vivo R_2 values are linearly linked to in-vivo R_2 values (Dawe et al., 2014). One limitation of the present work is that a single cerebral hemisphere was imaged for each participant and therefore any laterality differences as well as the association of R_2 with LATE-NC in commissural fibers, the brainstem and cerebellum were not investigated. A limitation of voxel-wise analyses in general is that inter-subject spatial normalization accuracy is lower in some parts of the cortex due to differences in cortical folding across people. Here, a state-of-the-art image registration method was used to reduce this problem (Avants et al., 2011).

5. Conclusion

The present MRI-pathology study in a large number of community-based older adults produced a novel spatial pattern for the independent association of lower R_2 values with higher LATE-NC stage. This pattern was consistent with the known distribution of LATE-NC in the brain of older adults and involved gray matter regions of the temporal, frontal, occipital lobes and basal ganglia, and white matter providing temporo-temporal, fronto-temporal, and temporo-basal ganglia connectivity. The extracted spatial pattern may be used in combination with other information (e.g. from other imaging modalities, biofluids etc.) to develop tools for in-vivo detection of this devastating disease process which, currently, can only be diagnosed at autopsy. Furthermore, in the present study, LATE-NC-related R_2 anomalies became statistically significant in stage 2 in the amygdala, hippocampus, parahippocampal white matter, and temporal pole white matter, and extended to more regions of the temporal, frontal, and occipital lobes, and basal ganglia in stage 3, suggesting that R_2 imaging may capture the general progression of LATE-NC, but the earliest impact of the pathology on R_2 is detected when TDP-43 inclusions extend beyond the amygdala. R_2 is one of the main sources of contrast in MRI, and to our knowledge this is the first study to investigate the R_2 signature of LATE-NC.

Acknowledgements

The authors are grateful to the participants and staff of the Rush University Memory and Aging Project, Religious Orders Study, and Minority Aging Research Study. This study was supported by the following grants from the National Institutes of Health: R01AG064233, R01AG067482, R01AG017917, R01AG015819, RF1AG022018, R01AG056405, R01AG052200, P30AG010161, P30AG072975 (National Institute on Aging), and UH2-UH3NS100599, UF1NS100599, R21NS076827 (National Institute of Neurological Disorders and Stroke).

Appendix A

Ex-vivo classification of LATE-NC based on regional R_2 values

Ex-vivo R_2 values in eight regions of interest (amygdala, hippocampus, parahippocampal white matter, temporal pole white matter, temporal lobe white matter, inferior insular white matter, medial orbitofrontal white matter, and occipitotemporal cortex) were used to build a linear support vector machine (SVM) classifier to distinguish LATE-NC stage 3 from earlier stages. First, regional R_2 values were adjusted for postmortem intervals and scanners, and then were centered by removing the mean and scaled to unit variance. To assess the

performance of the classifier, stratified shuffle split cross-validation was repeated 100 times, each time using 80% of the data for training and 20% for testing. Classifier hyperparameters were tuned using a grid search approach (10-fold cross-validation) on the training set of each repeat. The average area under the receiver operating characteristic curve (AUC) was computed. The average balanced accuracy, sensitivity, specificity, positive predictive value, and negative predictive value were also computed from the 100 repeats at classifier probability cut-off of 0.5.

The average AUC for ex-vivo classification of LATE-NC stage 3 based exclusively on regional R_2 was 0.70 (standard deviation, SD = 0.04) (Fig.A.1A). Additional metrics describing the performance of the classifier are summarized in Table A.1. These results indicate that R_2 can contribute towards prediction of LATE-NC, but additional information is needed to further improve performance.

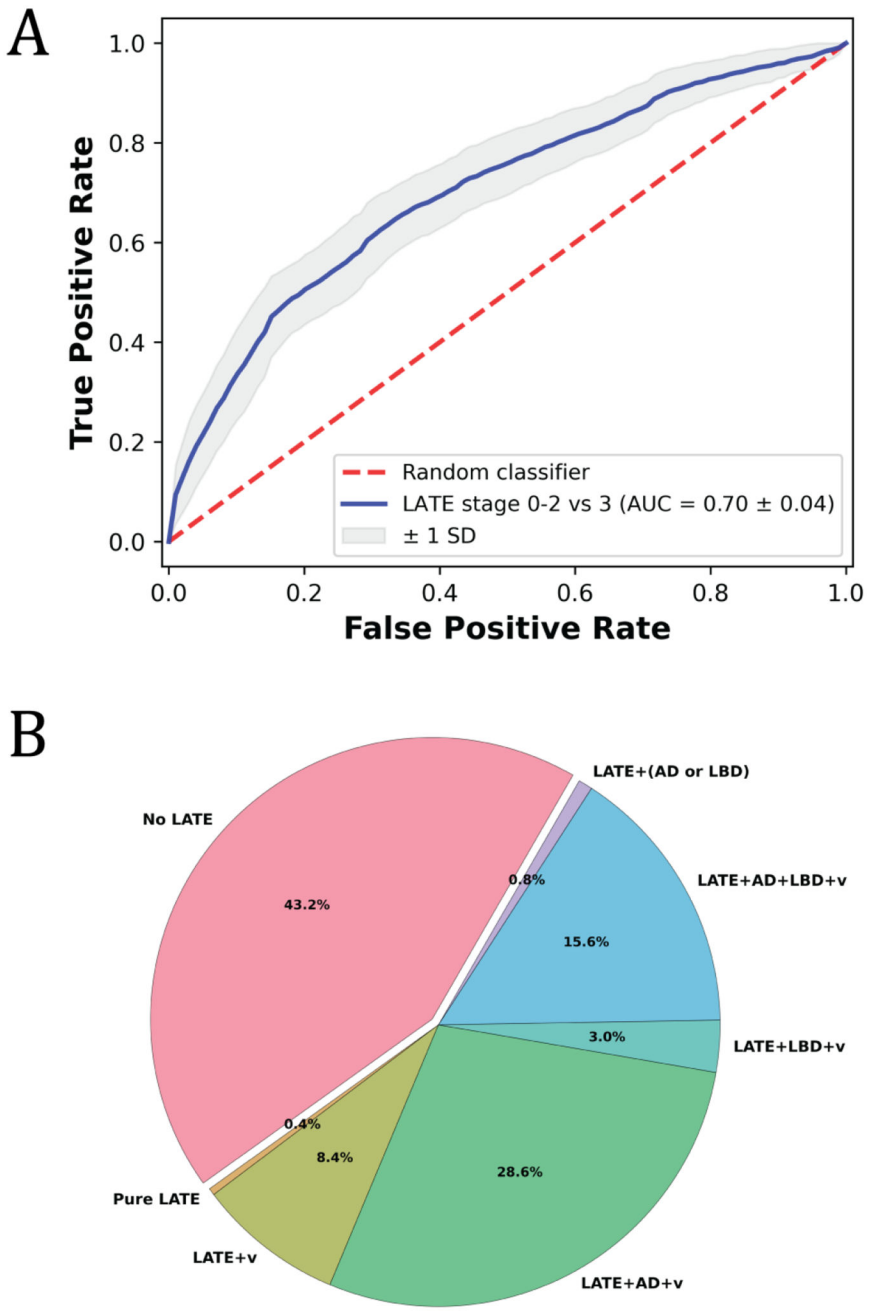

Figure A.1.

(A) Receiver operating characteristic curve for ex-vivo classification of LATE-NC stage 3 using an SVM classifier based exclusively on regional R_2 features. **(B)** Pie-chart illustrating the pathologies present in the participants that were considered in training and testing the classifier. Participants at LATE-NC stage 0 (no LATE-NC; but could have other pathologies) are represented by the pink slice, and participants with LATE-NC (stage ≥ 1) mixed with other neurodegenerative and vascular pathologies are represented by other colors (the abbreviation AD indicates intermediate or high AD neuropathological change according to NIA-AA; LBD indicates the presence of Lewy bodies; v indicates the presence

of vascular pathologies i.e. cerebral amyloid angiopathy, atherosclerosis, arteriolosclerosis, gross infarcts).

Table A.1.

Performance of an ex-vivo SVM classifier based exclusively on regional R_2

	AUC ± SD	Acc ± SD	PPV ± SD	NPV ± SD	Sens ± SD	Spec ± SD
LATE stage 0–2 vs 3	0.70 ± 0.04	0.65 ± 0.03	0.41 ± 0.03	0.84 ± 0.03	0.71 ± 0.06	0.59 ± 0.04

AUC, area under the receiver operating characteristics curve; SD, standard deviation; Acc, balanced accuracy; PPV, positive predictive value; NPV, negative predictive value; Sens, sensitivity; Spec, specificity

Abbreviations:

AD	Alzheimer's disease
AD-NC	AD neuropathological change
ANTs	advanced normalization tools
CAA	cerebral amyloid angiopathy
CERAD	Consortium to Establish a Registry for Alzheimer's Disease
FDG-PET	fluorodeoxyglucose positron emission tomography
FWER	familywise error rate
LATE-NC	limbic-predominant age-related TDP-43 encephalopathy neuropathological change
MAP	Rush Memory and Aging Project
MARS	Minority Aging Research Study
MCI	mild cognitive impairment
ME-SE	multi-echo spin-echo
MRI	magnetic resonance imaging
NCI	no cognitive impairment
NFT	Neurofibrillary tangles
NIA-AA	National Institute on Aging - Alzheimer's Association
PALM	permutation analysis of linear models
PMI_f	post-mortem interval to fixation
PMI_i	post-mortem interval to imaging
R_2	transverse relaxation rate constant

ROIs	region(s) of interest
ROS	Religious Orders Study
SD	standard deviation
T_2	transverse relaxation time constant
TDI	track density images
TDP-43	transactive response DNA binding protein of 43 kDa

References

Agrawal S, Yu L, Kapasi A, James BD, Arfanakis K, Barnes LL, Bennett DA, Nag S, Schneider JA, 2021a. Limbic-predominant age-related TDP-43 encephalopathy neuropathologic change and microvascular pathologies in community-dwelling older persons. Brain Pathol. 31, e12939. 10.1111/bpa.12939 [PubMed: 33624322]

Agrawal S, Yu L, Nag S, Arfanakis K, Barnes LL, Bennett DA, Schneider JA, 2021b. The association of Lewy bodies with limbic-predominant age-related TDP-43 encephalopathy neuropathologic changes and their role in cognition and Alzheimer's dementia in older persons. Acta Neuropathol. Commun. 2021 91 9, 1–11. 10.1186/S40478-021-01260-0

Amador-Ortiz C, Dickson DW, 2008. Neuropathology of Hippocampal Sclerosis. Handb. Clin. Neurol 10.1016/S0072-9752(07)01253-5

Amador-Ortiz C, Lin WL, Ahmed Z, Personett D, Davies P, Duara R, Graff-Radford NR, Hutton ML, Dickson DW, 2007. TDP-43 immunoreactivity in hippocampal sclerosis and Alzheimer's disease. Ann. Neurol 61, 435–445. 10.1002/ana.21154 [PubMed: 17469117]

Arai T, Mackenzie IRA, Hasegawa M, Nonoka T, Niizato K, Tsuchiya K, Iritani S, Onaya M, Akiyama H, 2009. Phosphorylated TDP-43 in Alzheimer's disease and dementia with Lewy bodies. Acta Neuropathol 117, 125–136. 10.1007/s00401-008-0480-1 [PubMed: 19139911]

Arfanakis K, Evia AM, Leurgans SE, Cardoso LFC, Kulkarni A, Alqam N, Lopes LF, Vieira D, Bennett DA, Schneider JA, 2020. Neuropathologic Correlates of White Matter Hyperintensities in a Community-Based Cohort of Older Adults. J. Alzheimer's Dis 73, 333–345. 10.3233/JAD-190687 [PubMed: 31771057]

Arnold SJ, Dugger BN, Beach TG, 2013. TDP-43 deposition in prospectively followed, cognitively normal elderly individuals: Correlation with argyrophilic grains but not other concomitant pathologies. Acta Neuropathol 126, 51–57. 10.1007/s00401-013-1110-0 [PubMed: 23604587]

Arvanitakis Z, Capuano AW, Leurgans SE, Bennett DA, Schneider JA, 2016. Relation of cerebral vessel disease to Alzheimer's disease dementia and cognitive function in elderly people: a cross-sectional study. Lancet Neurol 15, 934–943. 10.1016/S1474-4422(16)30029-1 [PubMed: 27312738]

Arvanitakis Z, Capuano AW, Leurgans SE, Buchman AS, Bennett DA, Schneider JA, 2017. The Relationship of Cerebral Vessel Pathology to Brain Microinfarcts. Brain Pathol 27, 77–85. 10.1111/bpa.12365 [PubMed: 26844934]

Avants BB, Tustison NJ, Song G, Cook PA, Klein A, Gee JC, 2011. A reproducible evaluation of ANTs similarity metric performance in brain image registration. Neuroimage 54, 2033–2044. 10.1016/j.neuroimage.2010.09.025 [PubMed: 20851191]

Barnes LL, Shah RC, Aggarwal NT, Bennett DA, Schneider JA, 2013. The Minority Aging Research Study: Ongoing Efforts to Obtain Brain Donation in African Americans without Dementia. Curr. Alzheimer Res 9, 734–745. 10.2174/156720512801322627

Bartzokis G, Cummings JL, Sultzer D, Henderson VW, Nuechterlein KH, Mintz J, 2003. White matter structural integrity in healthy aging adults and patients with Alzheimer disease: A magnetic resonance imaging study. Arch. Neurol 60, 393–398. 10.1001/archneur.60.3.393 [PubMed: 12633151]

Bejanin A, Murray ME, Martin P, Botha H, Tosakulwong N, Schwarz CG, Senjem ML, Chételat G, Kantarci K, Jack CR, Boeve BF, Knopman DS, Petersen RC, Giannini C, Parisi JE, Dickson

DW, Whitwell JL, Josephs KA, 2019. Antemortem volume loss mirrors TDP-43 staging in older adults with non-frontotemporal lobar degeneration. Brain 142, 3621–3635. 10.1093/brain/awz277 [PubMed: 31562527]

Bennett DA, Buchman AS, Boyle PA, Barnes LL, Wilson RS, Schneider JA, 2018. Religious Orders Study and Rush Memory and Aging Project. J. Alzheimer's Dis 10.3233/JAD-179939

Bennett DA, Schneider JA, Aggarwal N, Arvanitakis Z, Shah RC, Kelly JF, Fox JH, Cochran EJ, Arends D, Treinkman AD, Wilson RS, 2006. Decision rules guiding the clinical diagnosis of Alzheimer's disease in two community-based cohort studies compared to standard practice in a clinic-based cohort study. Neuroepidemiology 27, 169–176. 10.1159/000096129 [PubMed: 17035694]

Bennett DA, Wilson RS, Schneider JA, Evans DA, Beckett LA, Aggarwal NT, Barnes LL, Fox JH, Bach J, 2002. Natural history of mild cognitive impairment in older persons. Neurology 59, 198–205. 10.1212/WNL.59.2.198 [PubMed: 12136057]

Besson JAO, Best PV, Skinner ER, 1992. Post-mortem proton magnetic resonance spectrometric measures of brain regions in patients with a pathological diagnosis of Alzheimer's disease and multi-infarct dementia. Br. J. Psychiatry 160, 187–190. 10.1192/bjp.160.2.187 [PubMed: 1540758]

Boyle PA, Wilson RS, Aggarwal NT, Tang Y, Bennett DA, 2006. Mild cognitive impairment: Risk of Alzheimer disease and rate of cognitive decline. Neurology 67, 441–445. 10.1212/01.wnl.0000228244.10416.20 [PubMed: 16894105]

Boyle PA, Yu L, Nag S, Leurgans S, Wilson RS, Bennett DA, Schneider JA, 2015. Cerebral amyloid angiopathy and cognitive outcomes in community-based older persons. Neurology 85, 1930–1936. 10.1212/WNL.0000000000002175 [PubMed: 26537052]

Brown RW, Cheng YCN, Haacke EM, Thompson MR, Venkatesan R, 2014. Magnetic Resonance Imaging: Physical Principles and Sequence Design: Second Edition. Magn. Reson. Imaging Phys. Princ. Seq. Des Second Ed. 9780471720, 1–944. 10.1002/9781118633953

Buciuc M, Botha H, Murray ME, Schwarz CG, Senjem ML, Jones DT, Knopman DS, Boeve BF, Petersen RC, Jack CR, Petrucelli L, Parisi JE, Dickson DW, Lowe V, Whitwell JL, Josephs KA, 2020. Utility of FDG-PET in diagnosis of Alzheimer-related TDP-43 proteinopathy. Neurology 95, 23–34. 10.1212/WNL.0000000000009722

Dawe RJ, Bennett DA, Schneider JA, Arfanakis K, 2011. Neuropathologic correlates of hippocampal atrophy in the elderly: A clinical, pathologic, postmortem MRI study. PLoS One 6. 10.1371/journal.pone.0026286

Dawe RJ, Bennett DA, Schneider JA, Leurgans SE, Kotrotsou A, Boyle PA, Arfanakis K, 2014. Ex vivo T2 relaxation: Associations with age-related neuropathology and cognition. Neurobiol. Aging 35, 1549–1561. 10.1016/j.neurobiolaging.2014.01.144 [PubMed: 24582637]

Dawe RJ, Bennett DA, Schneider JA, Vasireddi SK, Arfanakis K, 2009. Postmortem MRI of human brain hemispheres: T2 relaxation times during formaldehyde fixation. Magn. Reson. Med 61, 810–818. 10.1002/mrm.21909 [PubMed: 19189294]

Dawe RJ, Yu L, Leurgans SE, Schneider JA, Buchman AS, Arfanakis K, Bennett DA, Boyle PA, 2016. Postmortem MRI: a novel window into the neurobiology of late life cognitive decline. Neurobiol. Aging 45, 169–177. 10.1016/j.neurobiolaging.2016.05.023 [PubMed: 27459937]

Fujishiro H, Uchikado H, Arai T, Hasegawa M, Akiyama H, Yokota O, Tsuchiya K, Togo T, Iseki E, Hirayasu Y, 2009. Accumulation of phosphorylated TDP-43 in brains of patients with argyrophilic grain disease. Acta Neuropathol 117, 151–158. 10.1007/s00401-008-0463-2 [PubMed: 19039597]

Geser F, Robinson JL, Malunda JA, Xie SX, Clark CM, Kwong LK, Moberg PJ, Moore EM, Van Deerlin VM, Lee VMY, Arnold SE, Trojanowski JQ, 2010. Pathological 43-kDa transactivation response DNA-binding protein in older adults with and without severe mental illness. Arch. Neurol 67, 1238–1250. 10.1001/archneurol.2010.254 [PubMed: 20937952]

Goedert M, Falcon B, Clavaguera F, Tolnay M, 2014. Prion-like mechanisms in the pathogenesis of tauopathies and synucleinopathies. Curr. Neurol. Neurosci. Rep 10.1007/s11910-014-0495-z

Haacke EM, Cheng NYC, House MJ, Liu Q, Neelavalli J, Ogg RJ, Khan A, Ayaz M, Kirsch W, Obenaus A, 2005. Imaging iron stores in the brain using magnetic resonance imaging. Magn. Reson. Imaging 23, 1–25. 10.1016/j.mri.2004.10.001 [PubMed: 15733784]

House MJ, St. Pierre TG, McLean C, 2008. 1.4T study of proton magnetic relaxation rates, iron concentrations, and plaque burden in Alzheimer's disease and control postmortem brain tissue. Magn. Reson. Med 60, 41–52. 10.1002/mrm.21586 [PubMed: 18523986]

Hyman BT, Phelps CH, Beach TG, Bigio EH, Cairns NJ, Carrillo MC, Dickson DW, Duyckaerts C, Frosch MP, Masliah E, Mirra SS, Nelson PT, Schneider JA, Thal DR, Thies B, Trojanowski JQ, Vinters HV, Montine TJ, 2012. National Institute on Aging-Alzheimer's Association guidelines for the neuropathologic assessment of Alzheimer's disease. Alzheimer's Dement 8, 1–13. 10.1016/j.jalz.2011.10.007 [PubMed: 22265587]

James BD, Wilson RS, Boyle PA, Trojanowski JQ, Bennett DA, Schneider JA, 2016. TDP-43 stage, mixed pathologies, and clinical Alzheimer's-type dementia. Brain 139, 2983–2993. 10.1093/brain/aww224 [PubMed: 27694152]

Josephs KA, Murray ME, Tosakulwong N, Weigand SD, Serie AM, Perkerson RB, Matchett BJ, Jack CR, Knopman DS, Petersen RC, Parisi JE, Petrucelli L, Baker M, Rademakers R, Whitwell JL, Dickson DW, 2019. Pathological, imaging and genetic characteristics support the existence of distinct TDP-43 types in non-FTLD brains. Acta Neuropathol 137, 227–238. 10.1007/s00401-018-1951-7 [PubMed: 30604226]

Josephs KA, Murray ME, Whitwell JL, Tosakulwong N, Weigand SD, Petrucelli L, Liesinger AM, Petersen RC, Parisi JE, Dickson DW, 2016. Updated TDP-43 in Alzheimer's disease staging scheme. Acta Neuropathol 131, 571–585. 10.1007/s00401-016-1537-1 [PubMed: 26810071]

Josephs KA, Whitwell JL, Weigand SD, Murray ME, Tosakulwong N, Liesinger AM, Petrucelli L, Senjem ML, Knopman DS, Boeve BF, Ivnik RJ, Smith GE, Jack CR, Parisi JE, Petersen RC, Dickson DW, 2014. TDP-43 is a key player in the clinical features associated with Alzheimer's disease. Acta Neuropathol 127, 811–824. 10.1007/s00401-014-1269-z [PubMed: 24659241]

Kawas C, Corrada M, 2006. Alzheimers and Dementia in the Oldest-Old: A Century of Challenges. Curr. Alzheimer Res 3, 411–419. 10.2174/156720506779025233 [PubMed: 17168640]

Kotrotsou A, Schneider JA, Bennett DA, Leurgans SE, Dawe RJ, Boyle PA, Golak T, Arfanakis K, 2015. Neuropathologic correlates of regional brain volumes in a community cohort of older adults. Neurobiol. Aging 36, 2798–2805. 10.1016/j.neurobiolaging.2015.06.025 [PubMed: 26195068]

Makkinejad N, Schneider JA, Yu J, Leurgans SE, Kotrotsou A, Evia AM, Bennett DA, Arfanakis K, 2019. Associations of amygdala volume and shape with transactive response DNA-binding protein 43 (TDP-43) pathology in a community cohort of older adults. Neurobiol. Aging 77, 104–111. 10.1016/j.neurobiolaging.2019.01.022 [PubMed: 30784812]

McAleese KE, Walker L, Erskine D, Thomas AJ, McKeith IG, Attems J, 2017. TDP-43 pathology in Alzheimer's disease, dementia with Lewy bodies and ageing. Brain Pathol 27, 472–479. 10.1111/bpa.12424 [PubMed: 27495267]

McKhann G, Drachman D, Folstein M, Katzman R, Price D, Stadlan EM, 1984. Clinical diagnosis of alzheimer's disease: Report of the NINCDS-ADRDA work group* under the auspices of department of health and human services task force on alzheimer's disease. Neurology 34, 939–944. 10.1212/wnl.34.7.939 [PubMed: 6610841]

Nag S, Yu L, Boyle PA, Leurgans SE, Bennett DA, Schneider JA, 2018. TDP-43 pathology in anterior temporal pole cortex in aging and Alzheimer's disease. Acta Neuropathol. Commun 6, 33. 10.1186/s40478-018-0531-3 [PubMed: 29716643]

Nag S, Yu L, Capuano AW, Wilson RS, Leurgans SE, Bennett DA, Schneider JA, 2015. Hippocampal sclerosis and TDP-43 pathology in aging and Alzheimer disease. Ann. Neurol 77, 942–952. 10.1002/ana.24388 [PubMed: 25707479]

Nelson PT, Dickson DW, Trojanowski JQ, Jack CR, Boyle PA, Arfanakis K, Rademakers R, Alafuzoff I, Attems J, Brayne C, Coyle-Gilchrist ITS, Chui HC, Fardo DW, Flanagan ME, Halliday G, Hokkanen SRK, Hunter S, Jicha GA, Katsumata Y, Kawas CH, Keene CD, Kovacs GG, Kukull WA, Levey AI, Makkinejad N, Montine TJ, Murayama S, Murray ME, Nag S, Rissman RA, Seeley WW, Sperling RA, White CL, Yu L, Schneider JA, 2019. Limbic-predominant age-related TDP-43 encephalopathy (LATE): Consensus working group report. Brain 10.1093/brain/awz099

Qi X, Arfanakis K, 2021. Regionconnect: Rapidly extracting standardized brain connectivity information in voxel-wise neuroimaging studies. Neuroimage 225. 10.1016/j.neuroimage.2020.117462

Schneider JA, Wilson RS, Cochran EJ, Bienias JL, Arnold SE, Evans DA, Bennett DA, 2003. Relation of cerebral infarctions to dementia and cognitive function in older persons. Neurology 60, 1082–1088. 10.1212/01.WNL.0000055863.87435.B2 [PubMed: 12682310]

Tremblay C, St-Amour I, Schneider J, Bennett DA, Calon F, 2011. Accumulation of transactive response DNA binding protein 43 in mild cognitive impairment and Alzheimer disease. J. Neuropathol. Exp. Neurol 10.1097/NEN.0b013e31822c62cf

Uchino A, Takao M, Hatsuta H, Sumikura H, Nakano Y, Nogami A, Saito Y, Arai T, Nishiyama K, Murayama S, 2015. Incidence and extent of TDP-43 accumulation in aging human brain. Acta Neuropathol. Commun 3, 35. 10.1186/s40478-015-0215-1 [PubMed: 26091809]

Wilson RS, Yu L, Trojanowski JQ, Chen EY, Boyle PA, Bennett DA, Schneider JA, 2013. TDP-43 pathology, cognitive decline, and dementia in old age. JAMA Neurol 70, 1418–1424. 10.1001/jamaneurol.2013.3961 [PubMed: 24080705]

Winkler AM, Ridgway GR, Webster MA, Smith SM, Nichols TE, 2014. Permutation inference for the general linear model. Neuroimage 92, 381–397. 10.1016/j.neuroimage.2014.01.060 [PubMed: 24530839]

Zarow C, Weiner MW, Ellis WG, Chui HC, 2012. Prevalence, laterality, and comorbidity of hippocampal sclerosis in an autopsy sample. Brain Behav 2, 435–442. 10.1002/brb3.66 [PubMed: 22950047]

Highlights

- Voxel-wise analysis showed a pattern of lower R_2 values for greater LATE-NC burden
- The pattern was consistent with the distribution of LATE-NC in gray matter
- The pattern also included white matter connections between regions with LATE-NC
- R_2 imaging may capture the general progression of LATE-NC
- R_2 becomes sensitive to LATE-NC when TDP-43 inclusions extend beyond the amygdala

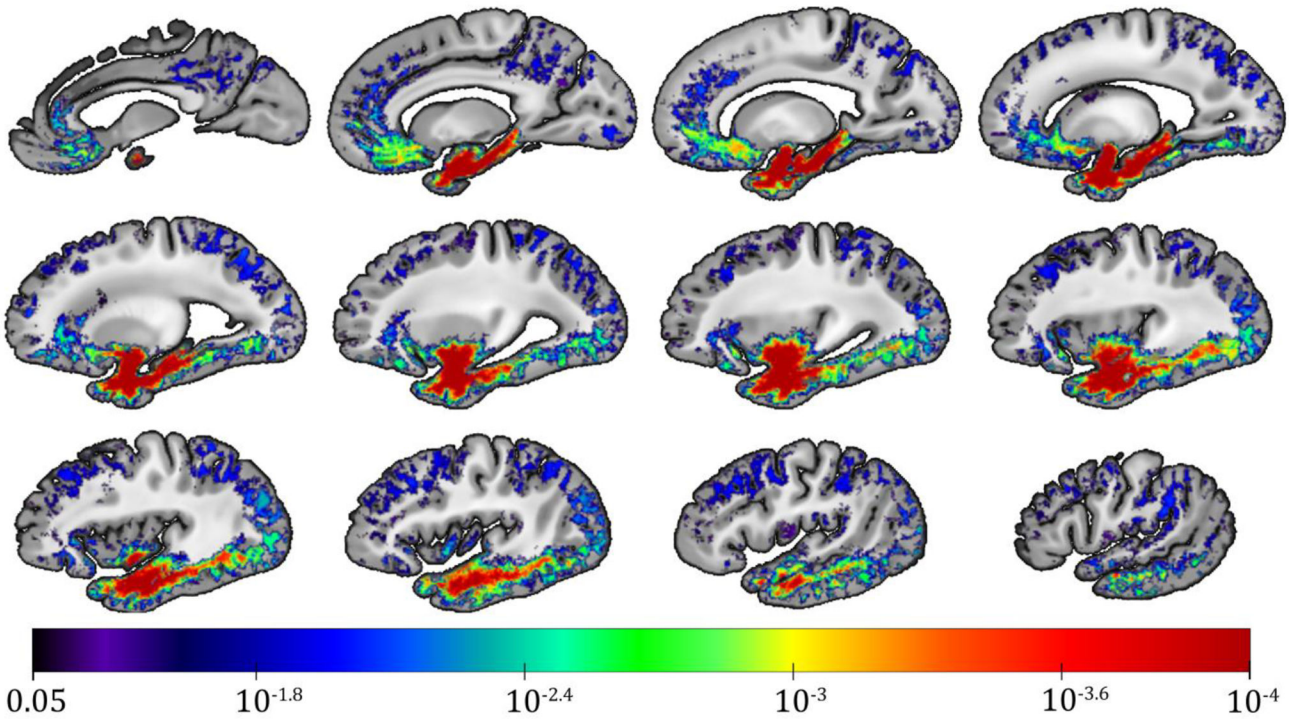

Figure 1.

Sagittal images arranged from medial (top left) to lateral (bottom right) showing regions in which the R_2 relaxation rate is significantly lower for higher LATE-NC stage according to voxel-wise linear regression that controlled for other neuropathologies, demographics and covariates. The color-scale represents the FWER-corrected p-values obtained from the voxel-wise linear regression, and the gray-scale images are showing the ex-vivo MRI brain hemisphere template used in this work.

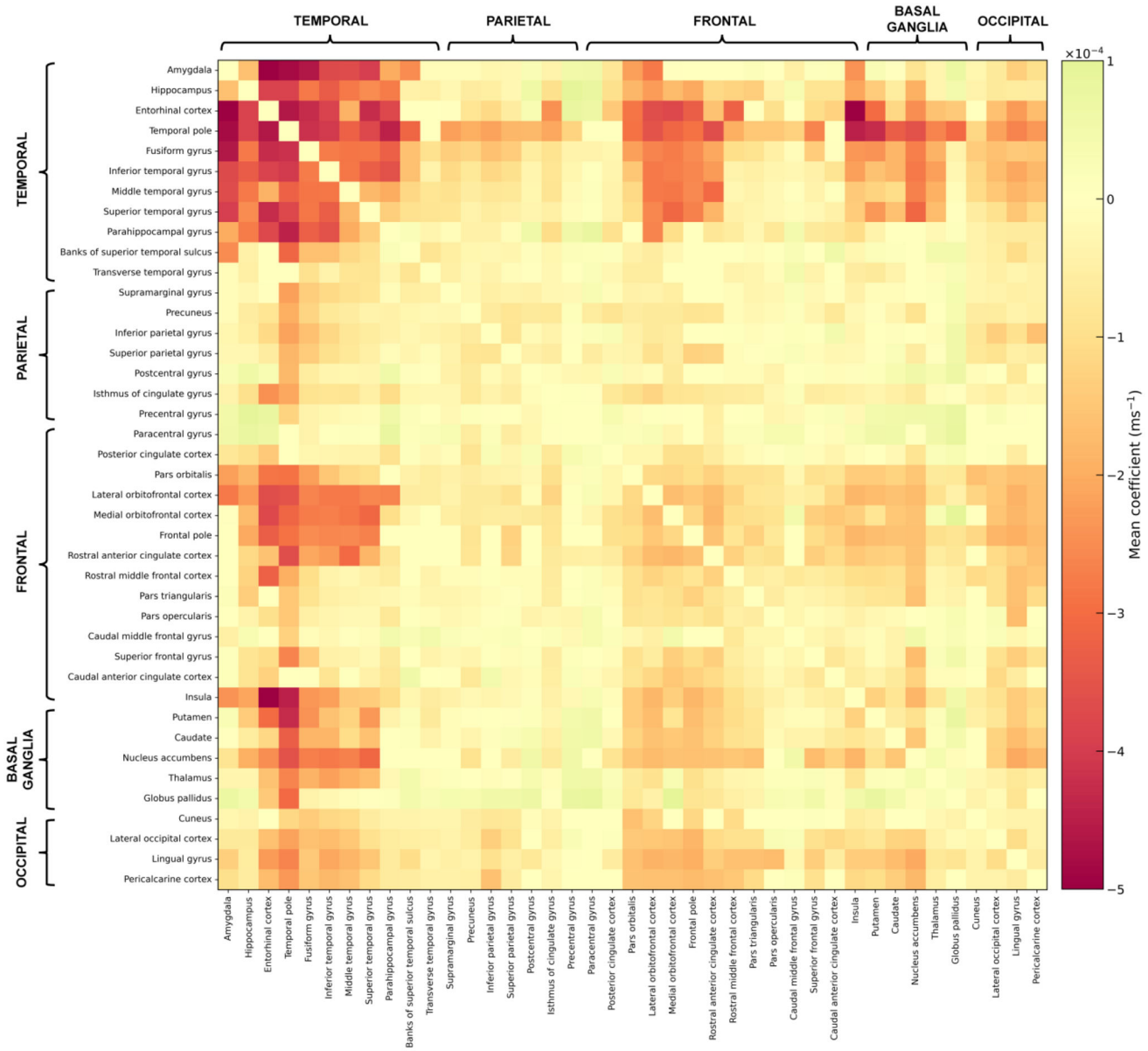

Figure 2.

Connectivity matrix showing the mean coefficient derived from the voxel-wise analysis on the association of R_2 with LATE-NC per connection of the structural connectome. Dark red colors represent the most negative associations of R_2 values with LATE-NC.

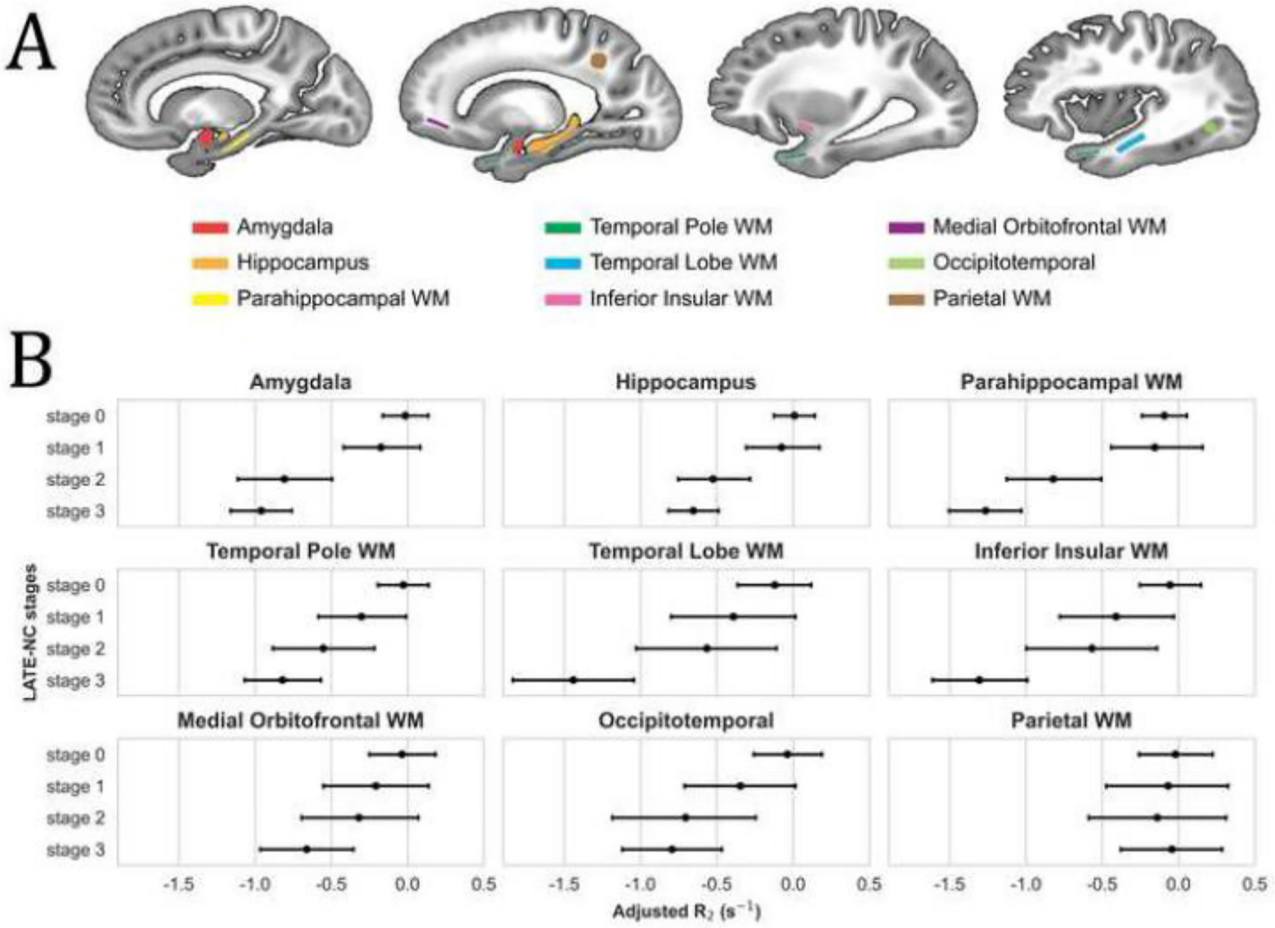

Fig. 3.

(A) Regions of interest (ROI) used in the investigation of R_2 differences in LATE-NC stages 1, 2, 3 compared to stage 0. WM stands for white matter. **(B)** Mean adjusted R_2 value and 95% confidence interval for each LATE-NC stage and each ROI. R_2 values have been adjusted for neuropathologies (other than LATE-NC), demographics, scanners, and postmortem intervals.

Table 1.

Demographic and clinical characteristics of the participants.

Characteristics	
N	738
Age at death, y (SD)	90.6 (6.4)
Male, n (%)	205 (27.8)
Education, y (SD)	15.7 (3.5)
Median time between last clinical evaluation and death, y	0.65
Antemortem clinical diagnosis[a]	
No cognitive impairment	226 (30.6)
Mild cognitive impairment	167 (22.6)
Dementia	345 (46.8)
Mini-Mental State Examination[a] (MMSE), mean (SD)	19.4 (9.7)
At least one copy of the ε4 allele, n (%)	199 (27.0)
Left hemisphere, n (%)	414 (56.1)
Postmortem interval to fixation, h (SD)	9.9 (7.8)
Postmortem interval to imaging, d (SD)	36.4 (15.9)
Scanner for ex vivo MRI, n (%)	
3T GE Signa	51 (6.9)
3T Siemens Trio	62 (8.4)
3T Philips Achieva	263 (35.6)
3T Siemens Verio	362 (49.1)

[a]Proximate to death

Table 2.

Neuropathologic characteristics of the participants.

Characteristics	
N	738
LATE-NC, n (%)	
(stage 0) no TDP-43 inclusions	319 (43.2)
(stage 1) TDP-43 inclusions in amygdala only	130 (17.6)
(stage 2) TDP-43 inclusions in amygdala and entorhinal cortex or hippocampus	81 (11)
(stage 3) TDP-43 inclusions in amygdala, entorhinal cortex or hippocampus, and neocortex	208 (28.2)
AD-NC (NIA-AA criteria), n (%)	
None	61 (8.2)
Low	132 (17.9)
Intermediate	346 (46.9)
High	199 (27)
Lewy bodies, n (%)	217 (29.4)
Gross infarcts, n (%)	298 (40.4)
Microscopic infarcts, n (%)	291 (39.4)
Cerebral amyloid angiopathy, n (%)	
None	145 (19.7)
Mild	324 (43.9)
Moderate	181 (24.5)
Severe	88 (11.9)
Atherosclerosis, n (%)	
None	174 (23.6)
Mild	394 (53.4)
Moderate	139 (18.8)
Severe	31 (4.2)
Arteriolosclerosis, n (%)	
None	273 (37)
Mild	277 (37.5)
Moderate	149 (20.2)
Severe	39 (5.3)

AD-NC, Alzheimer's Disease neuropathological change; LATE-NC, Limbic predominant age-related transactive response DNA binding protein 43 (TDP-43) encephalopathy neuropathological change; NIA-AA, National Institute on Aging-Alzheimer's Association.

Table 3.

Results of linear regression testing the hypothesis that regional R_2 values in LATE-NC stages 1, 2, 3 are lower than those in stage 0, controlling for other pathologies, demographics, scanners, and postmortem intervals.

Regions of Interest	LATE-NC Stage 1 vs. 0 β^a (p-value)	LATE-NC Stage 2 vs. 0 β^a (p-value)	LATE-NC Stage 3 vs. 0 β^a (p-value)	Arteriolosclerosis β^b (p-value)	Atherosclerosis β^b (p-value)	CAA β^b (p-value)	Gross infarcts β^b (p-value)	Lewy Bodies β^b (p-value)	A score β^b (p-value)	B score β^b (p-value)	C score β^b (p-value)
Amygdala	− 0.2 (0.46)	**− 0.8 (3×10^{-4})**	**− 0.9 (1×10^{-4})**	− 0.1 (0.15)	0 (0.86)	0.1 (0.06)	− 0.1 (0.46)	**− 0.4 (5×10^{-3})**	− 0.1 (0.54)	**− 0.4 (1×10^{-4})**	0 (0.84)
Hippocampus	− 0.1 (0.62)	**− 0.6 (3×10^{-3})**	**− 0.7 (1×10^{-4})**	− 0.1 (0.52)	0 (0.84)	**0.2 (0.03)**	− 0.1 (0.54)	− 0.2 (0.18)	− 0.2 (0.19)	**− 0.4 (1×10^{-4})**	0.1 (0.54)
Parahippocampal WM	− 0.1 (0.77)	**− 0.7 (1×10^{-3})**	**− 1.2 (1×10^{-4})**	0 (0.86)	0 (0.88)	**0.2 (0.04)**	− 0.1 (0.58)	**− 0.4 (0.02)**	0 (0.89)	**− 0.6 (1×10^{-4})**	− 0.1 (0.61)
Temporal Pole WM	− 0.3 (0.23)	**− 0.5 (0.03)**	**− 0.8 (1×10^{-4})**	0 (0.84)	0 (0.85)	0.1 (0.37)	− 0.1 (0.62)	− 0.1 (0.66)	0 (0.87)	**− 0.3 (0.04)**	− 0.2 (0.2)
Temporal Lobe WM	− 0.3 (0.47)	− 0.4 (0.39)	**− 1.3 (1×10^{-4})**	0 (0.83)	0 (0.81)	0 (0.85)	− 0.2 (0.2)	− 0.3 (0.37)	0.1 (0.8)	**− 0.8 (1×10^{-4})**	− 0.1 (0.62)
Insular WM	− 0.4 (0.22)	− 0.5 (0.17)	**− 1.2 (1×10^{-4})**	− 0.1 (0.69)	0 (0.83)	0.1 (0.33)	**− 0.4 (3×10^{-3})**	− 0.3 (0.23)	− 0.1 (0.57)	**− 0.5 (1×10^{-3})**	0 (0.88)
Medial Orbitofrontal WM	− 0.2 (0.6)	− 0.3 (0.53)	**− 0.6 (6×10^{-3})**	− 0.2 (0.14)	− 0.1 (0.49)	**0.3 (0.02)**	**− 0.4 (9×10^{-4})**	− 0.1 (0.6)	0.1 (0.76)	**− 0.5 (4×10^{-3})**	− 0.2 (0.15)
Occipitotemporal cortex	− 0.3 (0.4)	− 0.6 (0.11)	**− 0.7 (3×10^{-3})**	0 (0.84)	0.1 (0.72)	0 (0.87)	− 0.3 (0.07)	− 0.3 (0.36)	− 0.2 (0.33)	**− 0.8 (1×10^{-4})**	0.1 (0.72)
Parietal WM	− 0.1 (0.84)	− 0.1 (0.79)	0 (0.88)	− 0.2 (0.29)	0.2 (0.39)	**− 0.3 (0.04)**	**− 0.6 (1×10^{-4})**	− 0.2 (0.57)	0.1 (0.71)	**− 0.5 (3×10^{-3})**	0 (0.82)

CAA, cerebral amyloid angiopathy; WM, white matter

Statistically significant findings are shown in bold ($p<0.05$). FWER (family-wise error rate) corrected p-values are shown in parentheses.

[a] Coefficient denoting the difference in R_2 between two LATE-NC stages (units: sec^{-1})

[b] Coefficient denoting the difference in R_2 between consecutive levels of the pathology variable (units: sec^{-1})